

Dissociated functional significance of decision-related activity in the primate dorsal stream

Leor N. Katz^{1*}, Jacob L. Yates^{1*}, Jonathan W. Pillow² & Alexander C. Huk¹

During decision making, neurons in multiple brain regions exhibit responses that are correlated with decisions^{1–6}. However, it remains uncertain whether or not various forms of decision-related activity are causally related to decision making^{7–9}. Here we address this question by recording and reversibly inactivating the lateral intraparietal (LIP) and middle temporal (MT) areas of rhesus macaques performing a motion direction discrimination task. Neurons in area LIP exhibited firing rate patterns that directly resembled the evidence accumulation process posited to govern decision making^{2,10}, with strong correlations between their response fluctuations and the animal's choices. Neurons in area MT, in contrast, exhibited weak correlations between their response fluctuations and choices, and had firing rate patterns consistent with their sensory role in motion encoding¹. The behavioural impact of pharmacological inactivation of each area was inversely related to their degree of decision-related activity: while inactivation of neurons in MT profoundly impaired psychophysical performance, inactivation in LIP had no measurable impact on decision-making performance, despite having silenced the very clusters that exhibited strong decision-related activity. Although LIP inactivation did not impair psychophysical behaviour, it did influence spatial selection and oculomotor metrics in a free-choice control task. The absence of an effect on perceptual decision making was stable over trials and sessions and was robust to changes in stimulus type and task geometry, arguing against several forms of compensation. Thus, decision-related signals in LIP do not appear to be critical for computing perceptual decisions, and may instead reflect secondary processes. Our findings highlight a dissociation between decision correlation and causation, showing that strong neuron–decision correlations do not necessarily offer direct access to the neural computations underlying decisions.

We investigated the functional significance of decision-related activity by recording and inactivating neural activity in two well-studied cortical areas, MT and LIP, while rhesus monkeys performed a challenging motion discrimination task. On each trial, the monkey maintained stable visual fixation while discriminating the net direction of a visual motion stimulus, and then made a saccade to one of two choice targets to communicate their choice (Fig. 1a, b). For electrophysiological recordings in MT, we placed the motion stimulus in the receptive field of the neurons and aligned it with the preferred direction of one or more MT neurons on the multi-electrode array. For LIP, we placed one of the two targets in the response field of the neurons (as opposed to the visual motion stimulus), and the other target on the contralateral side of the visual field, consistent with previous studies of decision-related responses in LIP¹¹.

We recorded 157 MT neurons and 200 LIP neurons with either single electrodes or multi-electrode linear arrays. MT neurons that were well-targeted by the stimulus ($n = 94$) had average firing rates that depended on the motion strength and direction (Fig. 1c). As expected

in this area, responses increased sharply after motion onset and maintained a robust firing rate throughout motion viewing¹². The average responses of well-targeted LIP neurons ($n = 113$) were also consistent with classical observations^{2,11}, exhibiting ramp-like increases or decreases in firing rate, whose slopes were proportional to motion

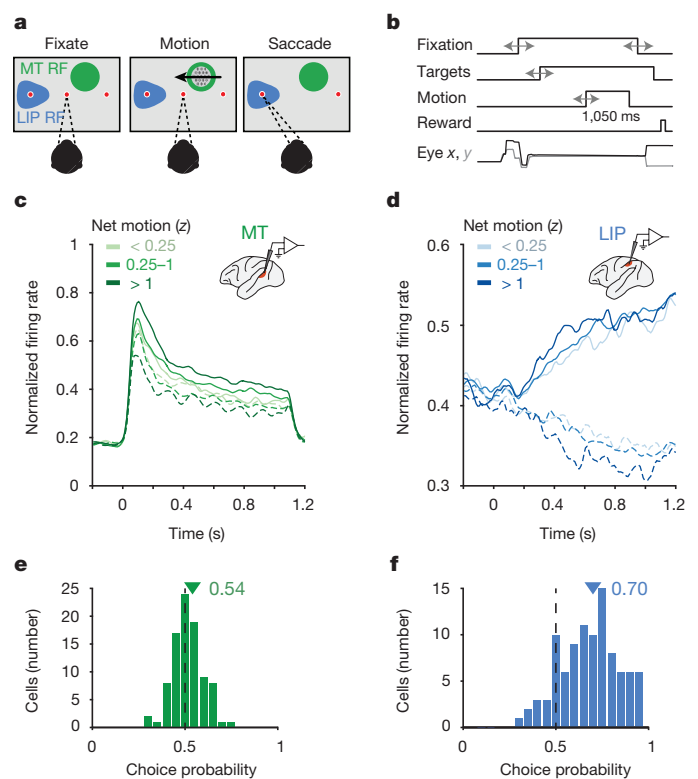


Figure 1 | Task and neural responses during direction discrimination.

a, Monkeys were trained to discriminate the direction of visual motion and communicate their decision with a saccadic eye movement to one of two choice targets. For MT recordings, motion was placed in the MT receptive field (RF) (green patch). For LIP recordings, one of the saccade targets was placed in the LIP receptive field (blue patch). **b**, Sequence of task events. Grey arrows indicate temporal jitter. **c**, Average response of 94 MT neurons as a function of motion strength (grouped by z -scored net motion, see Methods) and direction (preferred versus non-preferred direction, solid and dashed lines, respectively), aligned to motion onset. **d**, Average response of 113 LIP neurons as a function of motion strength and direction (in versus out of cell's receptive field, solid and dashed lines, respectively), aligned to motion onset. **e**, Choice probability for 90 MT neurons computed during the motion epoch. Triangle indicates mean, 0.54. **f**, Choice probability for 96 LIP neurons computed during the motion epoch. Triangle indicates mean, 0.70. Only neurons with >20 repeats of identical stimuli were included in the choice probability analysis.

¹Center for Perceptual Systems, Departments of Neuroscience & Psychology, The University of Texas at Austin, Austin, Texas 78712, USA. ²Princeton Neuroscience Institute & Department of Psychology, Princeton University, Princeton, New Jersey 08540, USA.

*These authors contributed equally to this work.

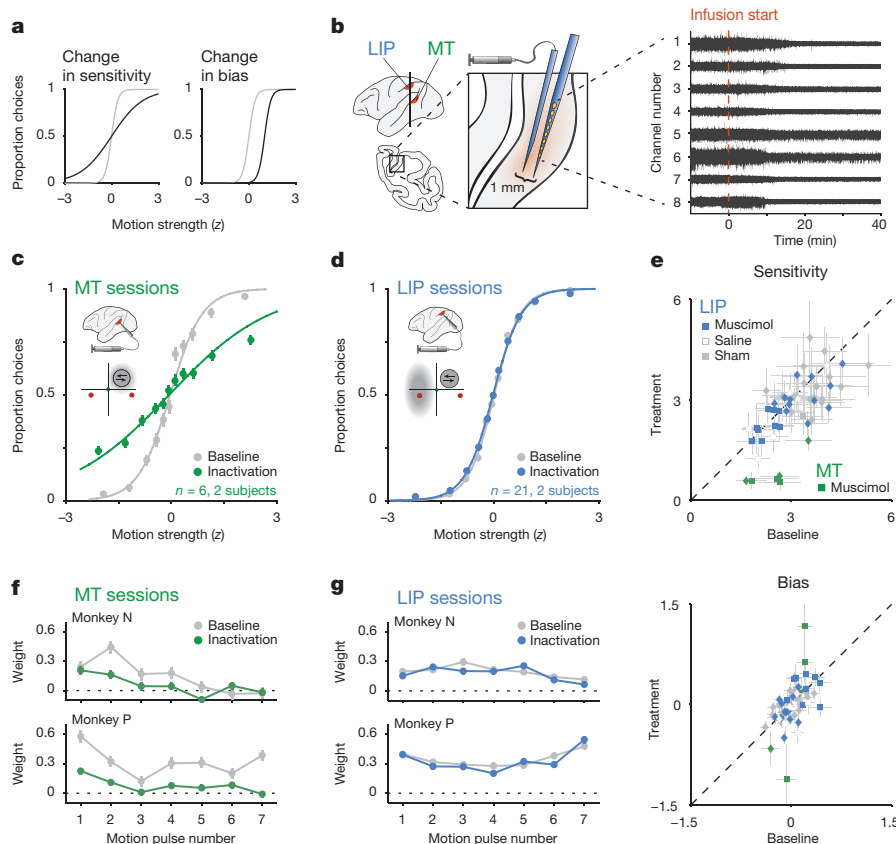


Figure 2 | Psychophysical performance before and after neural inactivations in areas MT and LIP. **a**, Hypothesized consequences of inactivation on the psychometric function. Left, decreased psychophysical sensitivity would correspond to a decrease in slope. Right, changes in psychophysical bias would correspond to a shifted midpoint. Positive values in the *x* axis (*z*-scored motion strength) refer to motion towards the target contralateral to the LIP under study. Correspondingly, the *y* axis refers to the proportion of contralateral target choices. This convention is maintained throughout. **b**, Schematic of the inactivation protocol. Left, a multi-electrode array was lowered alongside the cannula to identify the targeted cortical location, to verify neural selectivity before infusion, and to confirm neural silencing after. Right, continuous voltage traces from an example inactivation session in which neural silencing is evident ~10 min after infusion start. **c**, **d**, Psychophysical data for averaged pairs of baseline and muscimol treatment sessions in MT (**c**), and LIP (**d**). Insets illustrate

the brain region inactivated (top) and the corresponding experimental geometry (bottom), along with the estimated inactivated field (grey cloud). Error bars on points show ± 1 s.e.m. over all trials. **e**, The distribution of psychometric function parameters, slope (top) and shift (bottom), reflecting sensitivity and bias, respectively, for baseline (*x* axis) and treatment (*y* axis) session pairs for MT inactivations (green symbols), LIP inactivations (blue symbols), as well as LIP saline (open grey symbols) and sham/control experiments (filled grey symbols), for monkey N (diamonds) and monkey P (squares). Error bars show 95% confidence intervals for individual sessions. **f**, **g**, Psychophysical weighting, estimated via reverse correlation. The *y* axis indicates how much the subject weighed each of the motion stimulus pulses over all baseline and inactivation session pairs in MT (**f**) and in LIP (**g**), for monkey N (top) and monkey P (bottom). Error bars are s.e.m. over all trials.

strength, the primary physiological characteristic implicating LIP in reflecting the accumulation of evidence over time (Fig. 1d).

We further quantified the decision-related activity of MT and LIP using choice probability¹, a measure of correlation between neural activity and choices, independent of stimulus-driven responses. MT neurons were weakly but reliably correlated with the animal's choice on a trial-by-trial basis (mean choice probability = 0.54, $P = 1 \times 10^{-5}$; Fig. 1e). LIP neurons were more strongly correlated with choices (mean choice probability = 0.70, $P = 1 \times 10^{-21}$; Fig. 1f). Thus, the stimulus-dependent responses and choice probability in MT were consistent with its well-established role in representing the motion stimulus, and the response patterns in LIP resembled the time course of an evolving decision process. Together, these properties have given rise to a model where LIP neurons either integrate, or reflect the integration of, motion evidence from area MT in favour of a decision^{11,13}.

Having confirmed the neurophysiological properties of areas MT and LIP and their differential degrees of correlations with decisions, we tested their respective causal contributions by performing reversible inactivations in each area and evaluating the impacts on psychophysical performance (hypothesized outcomes shown in Fig. 2a). We infused muscimol (a GABA_A agonist which hyperpolarizes cell

bodies but not fibres of passage¹⁴) into either MT or LIP, 1 mm away from a multi-electrode array (Fig. 2b). The injection cannula was targeted to locations that had yielded the largest number of canonical MT or LIP units during recording sessions (Extended Data Fig. 1). The multi-electrode array was used to confirm both pre-infusion physiological properties and post-infusion neural silencing, performed on every inactivation session. Silencing was typically observed across all recording channels of the array (Fig. 2b) and estimated to span a spherical volume of ~2.5 mm radius (see Methods).

Inactivations in area MT exerted large effects on psychophysical performance. The motion stimulus was placed within a region of visual space retinotopically matched to the inactivated population of MT neurons (Fig. 2c). MT inactivations ($n = 6$; 3 in monkey N; 3 in monkey P) had a large and consistent impact on direction discrimination sensitivity (68.5% reduction from baseline, $t_{(5)} = -9.7$, $P = 0.002$, paired *t*-test). When the motion stimulus was moved outside the inactivated region within the same session ($n = 3$), psychophysical performance was restored, confirming that the effects were not due to general changes in arousal or vigilance (Extended Data Fig. 2). These severe and specific impairments in direction discrimination performance were consistent with prior causal perturbations^{15,16}.

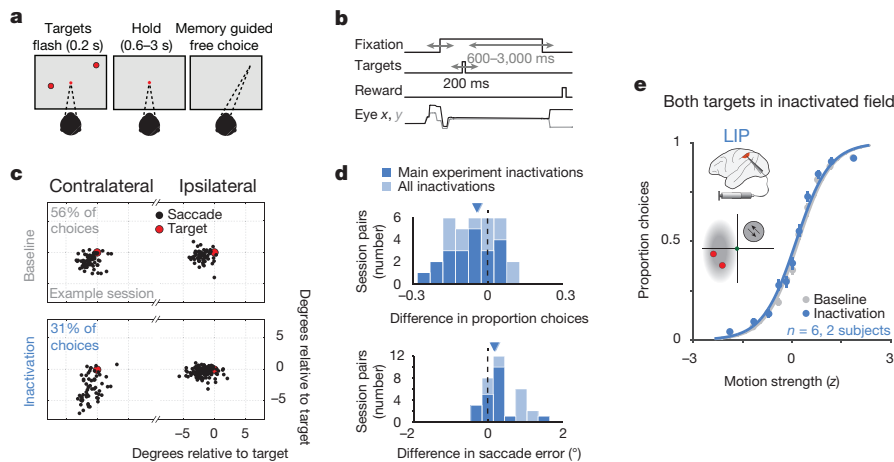


Figure 3 | Performance in control tasks following LIP inactivation.

a, Structure of the free-choice task. Following a 200-ms long presentation of two targets at random locations in space, monkeys were required to hold fixation for another 600–3,000 ms, and then to move their eyes to the remembered location of either target. **b**, Event timing in the free-choice task. Events in the task were presented in sequence and were jittered in time (grey arrows). **c**, The effect of LIP inactivation on choice bias and saccade accuracy in the free-choice task (example session). Saccade landing points (black dots) have been aligned to target position (red dot), for contralateral (left) and ipsilateral target choices (right), during baseline (top) and inactivation (bottom). Both saccadic accuracy and percent contralateral choices (indicated, top left) are reduced after LIP inactivation, to the contralateral hemifield. **d**, The effect of LIP inactivation on choice bias and saccade accuracy in the free-choice task,

over all sessions. Histograms show baseline/inactivation differences in proportion contralateral choices (top) and saccade error (bottom), where positive numbers indicate an increase in metric following inactivation. Dark bars indicate sessions that took place on the same days as the main direction discrimination experiment (main experiment inactivations, $n = 21$; 12 in monkey N; 9 in monkey P); dark triangle indicates the median difference. Light bars include an additional 13 sessions that took place during other inactivation experiments under similar conditions (all inactivations, $n = 34$; 14 in monkey N; 20 in monkey P); light triangle indicates median difference (visually occluded by dark triangle). **e**, Psychophysical data for pairs of baseline and muscimol treatment in LIP when both choice targets were placed within the inactivated field. Inset presents stimulus geometry and estimated inactivated field. Error bars are s.e.m. over all trials.

In contrast, inactivations in area LIP ($n = 21$; 12 in monkey N; 9 in monkey P) did not exert compelling or substantial effects on psychophysical performance (Fig. 2d). In these experiments, we placed one choice target in the inactivated region of visual space, consistent with previous electrophysiological investigations that placed a choice target (and not the visual motion stimulus) in the response fields of LIP neurons to elicit the area's canonical decision-related responses. Although we performed large inactivations in locations where LIP electrophysiology had mirrored the accumulation of evidence and demonstrated strong decision-related activity, we did not detect significant changes in either the animal's sensitivity or bias, as indicated by statistically indistinguishable differences in the slope (3.7% reduction from baseline, $t_{(20)} = -1.4$, $P = 0.16$, paired t -test) or midpoint (-0.4% shift, $t_{(20)} = -0.08$, $P = 0.93$, paired t -test) of the psychometric functions. Saline and sham control experiments showed similar patterns to the main baseline versus muscimol treatment comparison (Extended Data Table 1). Thus, although the effect of MT inactivation on sensitivity was substantial, an effect of LIP inactivation was not clearly identifiable using our techniques and task (Fig. 2e).

We also assessed whether inactivation affected the timing or strategy of evidence integration^{8,17,18}. For example, if LIP supported the temporal integration of motion evidence, inactivation could alter the strategy to reflect 'leakier' integration that might still support the same overall performance. Contrary to this possibility, inactivation in LIP did not lead to greater reliance on either early or late information (Fig. 2f, g), as estimated via reverse correlation. Inactivations in area MT, in contrast, reduced the psychophysical weighting of motion roughly evenly over time.

Although inactivation in LIP had no measurable effect on direction discrimination, it did exert effects on a 'free-choice' control task, which was performed on every inactivation session (Fig. 3a, b). LIP inactivation biased choices away from the contralateral hemifield (8.88% reduction from baseline on average, $t_{(33)} = 3.4$, $P = 0.001$, paired t -test), (Fig. 3c, d), consistent with previous reports in monkeys^{19–21}, rodents⁸, and parietal lesions in humans²². Thus, our electrophysiological

confirmation of LIP inactivation was complemented by a behavioural consequence in this free-choice control task. In addition to causing a spatial choice bias, LIP inactivation led to an increase in endpoint error of saccades made to the hemifield contralateral to inactivation (0.36° on average, $t_{(33)} = 4.4$, $P = 7 \times 10^{-5}$, Fig. 3c, d). No systematic change was detected in other oculomotor metrics during the free-choice task (reaction time, peak velocity, or duration), and no effects on any oculomotor metrics were detected during the direction discrimination task. Despite observing a muscimol-induced effect in the free-choice task, effect magnitude in the free-choice task was not predictive of effect magnitude in the direction discrimination task (Extended Data Fig. 3a, b), nor was there a dose–response relationship between muscimol mass and behavioural performance (Extended Data Fig. 3c–e), suggesting that our large muscimol administrations were probably operating within a 'ceiling' regime.

Because muscimol inactivations require comparisons across relatively long time scales, it remains logically possible that LIP normally plays a critical role in decision making, given that other areas are processing information in parallel and are able to quickly compensate when it is artificially inactivated. Although other techniques with faster time scales will allow for more direct tests of this possibility, we did not observe changes indicative of compensation either within a session or over sessions (Extended Data Figs 4 and 5, respectively). We also tested for compensation involving the non-inactivated hemisphere²³. We performed 6 additional inactivation experiments with both choice targets placed in a single hemifield (Fig. 3e, inset), in order to maximize reliance on a single hemisphere's LIP and hence minimize involvement of the other hemisphere. Inactivation of the LIP corresponding to the two targets did not produce clear changes in behavioural performance (Fig. 3e), indicating that inter-hemispheric compensation was unlikely in our main experiments. Previous LIP inactivation studies also find no evidence in support of compensation that manifests behaviourally (see the section on spatial and temporal extent of inactivation in the Methods). We also found no disruption of decision-making performance using the moving-dot stimulus used in

previous studies of MT and LIP function during decision making^{2,15} (Extended Data Fig. 6c).

Our results reveal a dissociation between decision-related activity in LIP and the causal role of such activity in decision making. Instead, decision-related signals in LIP may be a result of feedback²⁴, or an emergent phenomenon driven by extensive training²⁵. Although one prior study observed effects of LIP microstimulation in a reaction time direction discrimination task²⁶, such electrical perturbations can produce orthodromic (and antidromic) activation of connected areas, and their observed effects are reconcilable with multiple alternatives to evidence accumulation⁶. It remains possible that LIP contributes to decision making in conjunction with associated brain regions, whose parallel and/or redundant processing simply renders LIP unnecessary in the particular tasks used to study its decision-related activity. Indeed, a growing body of work has observed decision-related activity in other brain areas^{3–6,9}, consistent with the prospect of LIP playing a minor and/or nonessential role in decision making. Our results mirror findings in rodent posterior parietal cortex, where inactivations did not affect decision making despite electrophysiological correlates of evidence accumulation⁸. Finally, a richer appreciation of LIP's contributions to decision making might be gleaned from placing the motion stimulus itself (as opposed to the saccadic choice target) within the inactivated field, a configuration studied electrophysiologically in a categorization task²⁷, but not yet causally investigated.

Decision-related activity is probably represented broadly across the brain, and may be read out by a flexible process to support behaviour in LIP, or elsewhere^{7,18,28}. Our results call for a broader consideration of decision-making circuitry and more nuanced mechanisms for reading out decision-related activity—regardless of whether decisions are conveniently reflected, or actually computed, in the activity of a particular brain area^{23,29,30}.

Online Content Methods, along with any additional Extended Data display items and Source Data, are available in the online version of the paper; references unique to these sections appear only in the online paper.

Received 25 February; accepted 31 May 2016.

Published online 4 July 2016.

- Britten, K. H., Newsome, W. T., Shadlen, M. N., Celebri, S. & Movshon, J. A. A relationship between behavioral choice and the visual responses of neurons in macaque MT. *Vis. Neurosci.* **13**, 87–100 (1996).
- Shadlen, M. N. & Newsome, W. T. Neural basis of a perceptual decision in the parietal cortex (area LIP) of the rhesus monkey. *J. Neurophysiol.* **86**, 1916–1936 (2001).
- Gu, Y., DeAngelis, G. C. & Angelaki, D. E. A functional link between area MSTd and heading perception based on vestibular signals. *Nature Neurosci.* **10**, 1038–1047 (2007).
- Ding, L. & Gold, J. I. The basal ganglia's contributions to perceptual decision making. *Neuron* **79**, 640–649 (2013).
- Liu, S., Gu, Y., DeAngelis, G. C. & Angelaki, D. E. Choice-related activity and correlated noise in subcortical vestibular neurons. *Nature Neurosci.* **16**, 89–97 (2013).
- Hanks, T. D. *et al.* Distinct relationships of parietal and prefrontal cortices to evidence accumulation. *Nature* **520**, 220–223 (2015).
- Pitkow, X., Liu, S., Angelaki, D. E., DeAngelis, G. C. & Pouget, A. How can single sensory neurons predict behavior? *Neuron* **87**, 411–423 (2015).
- Erich, J. C., Brunton, B. W., Duan, C. A., Hanks, T. D. & Brody, C. D. Distinct effects of prefrontal and parietal cortex inactivations on an accumulation of evidence task in the rat. *eLife* **4**, 8166 (2015).
- Cumming, B. G. & Nienborg, H. Feedforward and feedback sources of choice probability in neural population responses. *Curr. Opin. Neurobiol.* **37**, 126–132 (2016).
- Brunton, B. W., Botvinick, M. M. & Brody, C. D. Rats and humans can optimally accumulate evidence for decision-making. *Science* **340**, 95–98 (2013).
- Gold, J. I. & Shadlen, M. N. The neural basis of decision making. *Annu. Rev. Neurosci.* **30**, 535–574 (2007).
- Britten, K. H., Shadlen, M. N., Newsome, W. T. & Movshon, J. A. Responses of neurons in macaque MT to stochastic motion signals. *Vis. Neurosci.* **10**, 1157–1169 (1993).
- Mazurek, M. E., Roitman, J. D., Ditterich, J. & Shadlen, M. N. A role for neural integrators in perceptual decision making. *Cereb. Cortex* **13**, 1257–1269 (2003).
- Hess, R. & Murata, K. Effects of glutamate and GABA on specific response properties of neurones in the visual cortex. *Exp. Brain Res.* **21**, 285–297 (1974).
- Newsome, W. T. & Paré, E. B. A selective impairment of motion perception following lesions of the middle temporal visual area (MT). *J. Neurosci.* **8**, 2201–2211 (1988).
- Chowdhury, S. A. & DeAngelis, G. C. Fine discrimination training alters the causal contribution of macaque area MT to depth perception. *Neuron* **60**, 367–377 (2008).
- Kiani, R., Hanks, T. D. & Shadlen, M. N. Bounded integration in parietal cortex underlies decisions even when viewing duration is dictated by the environment. *J. Neurosci.* **28**, 3017–3029 (2008).
- Raposo, D., Kaufman, M. T. & Churchland, A. K. A category-free neural population supports evolving demands during decision-making. *Nature Neurosci.* **17**, 1784–1792 (2014).
- Wardak, C., Olivier, E. & Duhamel, J.-R. A deficit in covert attention after parietal cortex inactivation in the monkey. *Neuron* **42**, 501–508 (2004).
- Balan, P. F. & Gottlieb, J. Functional significance of nonspatial information in monkey lateral intraparietal area. *J. Neurosci.* **29**, 8166–8176 (2009).
- Wilke, M., Kagan, I. & Andersen, R. A. Functional imaging reveals rapid reorganization of cortical activity after parietal inactivation in monkeys. *Proc. Natl Acad. Sci. USA* **109**, 8274–8279 (2012).
- Kerckhoff, G. Spatial hemineglect in humans. *Prog. Neurobiol.* **63**, 1–27 (2001).
- Li, N., Daie, K., Svoboda, K. & Druckmann, S. Robust neuronal dynamics in premotor cortex during motor planning. *Nature* **532**, 459–464 (2016).
- Crowe, D. A. *et al.* Prefrontal neurons transmit signals to parietal neurons that reflect executive control of cognition. *Nature Neurosci.* **16**, 1484–1491 (2013).
- Sarma, A. N., Masse, N. Y., Wang, X.-J. & Freedman, D. J. Task-specific versus generalized mnemonic representations in parietal and prefrontal cortices. *Nature Neurosci.* **19**, 143–149 (2016).
- Hanks, T. D., Ditterich, J. & Shadlen, M. N. Microstimulation of macaque area LIP affects decision-making in a motion discrimination task. *Nature Neurosci.* **9**, 682–689 (2006).
- Freedman, D. J. & Assad, J. A. Experience-dependent representation of visual categories in parietal cortex. *Nature* **443**, 85–88 (2006).
- Siegel, M., Buschman, T. J. & Miller, E. K. Cortical information flow during flexible sensorimotor decisions. *Science* **348**, 1352–1355 (2015).
- Heitz, R. P. & Schall, J. D. Neural chronometry and coherency across speed-accuracy demands reveal lack of homomorphism between computational and neural mechanisms of evidence accumulation. *Phil. Trans. R. Soc. B* **368**, 20130071 (2013).
- Mante, V., Sussillo, D., Shenoy, K. V. & Newsome, W. T. Context-dependent computation by recurrent dynamics in prefrontal cortex. *Nature* **503**, 78–84 (2013).

Acknowledgements We thank R. Krauzlis, C. Brody, E. Seidemann, L. Cormack, and R. Aldrich for comments on the manuscript. We thank the Brody laboratory (particularly C. Brody and J. Erlich) for inspiring the experiments, the Mauk laboratory (particularly M. Mauk, F. Riusech, and H. Halverson) for assistance with muscimol preparation, and K. Mitchell for animal support. This research was supported by the Howard Hughes Medical Institute International Student Research Fellowship to L.N.K., the McKnight Foundation grant to J.W.P., the National Eye Institute (R01-EY017366) grant to both J.W.P. and A.C.H., and the National Institutes of Health under Ruth L. Kirschstein National Research Service Awards T32DA018926 from the National Institute on Drug Abuse and T32EY021462 from the National Eye Institute.

Author Contributions L.N.K., J.L.Y. and A.C.H. designed the experiments. L.N.K. and J.L.Y. collected behavioural and electrophysiological data. L.N.K. and J.L.Y. performed pharmacological inactivations. L.N.K. analysed behavioural data. J.L.Y. analysed electrophysiological data. J.W.P. and A.C.H. guided data analysis. All authors discussed the results and wrote the manuscript.

Author Information Reprints and permissions information is available at www.nature.com/reprints. The authors declare no competing financial interests. Readers are welcome to comment on the online version of the paper. Correspondence and requests for materials should be addressed to L.N.K. (leor.katz@utexas.edu).

METHODS

Monkey preparation. We performed electrophysiological recordings and reversible inactivations in the MT and the LIP cortices of two rhesus macaques (subject N and subject P), female and male, aged 10 and 14 years, weighing 7.7 and 10 kg, respectively. Subject N had a custom titanium chamber that enabled access to both MT and LIP on the right hemisphere (L9, P2), guided by MRI. Subject P had a cilux chamber (Crist Instruments) over the right LIP (L12, P5) and another over the left V1 for a posterior approach to MT (L17, P17). Standard surgical procedures were applied³¹. All experimental protocols were approved by The University of Texas Institutional Animal Care and Use Committee and in accordance with National Institute of Health standards for care and use of laboratory animals.

The subject sat comfortably while head-posted in a primate chair (Crist Instruments), facing a linearized 55 inch LCD (LG) monitor (resolution = 1,920 × 1,080 pixels, refresh rate = 60 Hz, background luminance = 26.49 cd m⁻²) at a distance of 118 cm, in a dark room. Eye position was recorded using an Eyelink 1000 eye tracker (SR Research), sampled at 1 kHz. A solenoid-operated reward system was used to deliver liquid reward to the monkey. Stimuli were generated by using the Psychophysics Toolbox³² in MATLAB (MathWorks), and task events and neural responses were recorded (Plexon) using a Datapixx I/O box (Vpixx) for precise temporal registration. All of these systems were integrated using the PLDAPS system³³.

General procedure and experimental design. Recording sessions in either MT or LIP began by lowering an electrode to the known location of the area based on previous mapping and recording sessions. Anatomical identification (MR guided in monkey N; previously established in monkey P³¹) was followed by functional identification (mapping receptive/response fields of MT and LIP neurons, detailed below). Inactivations of either area began by lowering both a cannula and multi-channel electrode array to the region of interest, collaterally, at least 1 mm apart. The electrode array was used to (i) confirm that the cannula was within the target cortex, (ii) to record electrophysiological responses to relevant task events pre-infusion, and (iii) to confirm the electrophysiological silencing of neurons during and after the infusion. Thus, while it is not feasible to precisely measure the inactivated proportion of an area, we do confirm the silencing of a large swath (approximately 2.5 mm in radius), on every session (detailed in infusion protocol section, below).

MT inactivation was predicted to disrupt motion direction discrimination sensitivity within a specific region of contralateral space, consistent with MT retinotopic organization^{15,16}. The behavioural consequence of MT inactivation was measured by comparing psychophysical performance in the direction-discrimination task, before and after muscimol infusion, within the same experimental session, with the motion stimulus placed inside the inactivated region of space. LIP inactivation was predicted to disrupt spatial selection to contralateral space more generally^{8,19–21,34,35}, noting that LIP receptive fields are large and that the topographic organization is less precise than in earlier visual areas³⁶. The behavioural consequence of LIP inactivation was measured by comparing the proportion of contralateral choices in a double-target memory-guided free-choice task, before and after muscimol infusion, within the same session. To measure the effect of LIP inactivation in the direction-discrimination task, we compared psychophysical performance between pairs of sessions, baseline and treatment, in which the treatment session was a muscimol, saline, or sham infusion treatment. The paired sessions typically took place one day apart at the same time of day, and after a similar number of tasks and trials, to minimize the impact of within-session fatigue or motivation on behaviour. Behavioural data were collected 15–30 min after muscimol/saline/sham infusion end, and were always completed within 150 min. An additional 16 control pairs (without saline or sham manipulation) were collected to better estimate session-to-session variability. Statistical results do not depend on the inclusion/exclusion of these control session pairs. The number of paired sessions (Extended Data Fig. 6c and Extended Data Table 2) was chosen to match or exceed that in similar inactivation studies. The experiments were not randomized, and the investigators were not blinded to the experimental conditions.

Direction discrimination task. The principal task was a motion direction discrimination task. Subjects were required to discriminate the net direction of a motion stimulus and communicate their decision with an eye movement to one of two targets. The sequence of task events is presented in Fig. 1a. The timing of each event was randomly jittered from trial to trial (Fig. 1b). A trial began with the appearance of a fixation point. Once the monkey acquired fixation and held for 400–1,200 ms (uniform distribution), two targets appeared and remained visible until the end of the trial. 200–1,000 ms after target onset, the motion stimulus was presented at an eccentricity of 5–7° for 1,050 ms. The fixation point was extinguished 200–1,000 ms after motion offset, and the subject was required to shift

its gaze towards one of the two targets within 600 ms (saccade end points within 3° of the target location were accepted).

We used a reverse-correlation motion stimulus inspired by the classic moving-dot stimulus¹⁵ in which motion was in either one direction or the opposite, with varying motion strength. The motion stimulus consisted of 19 non-overlapping Gabor elements arranged in a hexagonal grid (5–7° across, scaled by eccentricity). The individual elements were set to approximate the receptive field size of a V1 neuron and the entire motion stimulus approximated the receptive field size of an MT neuron. Motion was presented by varying the phase of the sine-wave carrier of the Gabors. Each Gabor underwent a sinusoidal contrast modulation with independent random phase to prevent perceptual ‘pop-out’ of individual drifting elements. Gabor spatial frequency (0.9 cycles per °, $\sigma = 0.1 \times \text{eccentricity}$) and temporal frequency (7 Hz for monkey N, 5 Hz for monkey P, yielding velocities of 7.77 and 5.55° per s, respectively) were selected to match the approximate sensitivity of MT neurons.

Each trial comprised seven consecutive motion pulses lasting 150 ms each (9 video frames), producing a pulse sequence of 1,050 ms in duration. On any given pulse X_i , a number of Gabors would have their carrier sine waves drift in unison to produce motion (‘signal’ Gabors), and the remaining would counter-phase flicker (‘noise’ Gabors). Signal Gabors on pulse X_i were assigned at random within the grid and all signal Gabors drifted in the same direction.

Motion strength was defined as the proportion of signal Gabors out of the total, the value of which was drawn from a Gaussian distribution, $X_i \sim N(\mu_k, \sigma)$ and rounded to the nearest integer, where μ_k was set to one of five values at random: -50%, -12%, 0%, 12%, and 50% (negative sign indicates motion in the opposite direction), and σ was set to 15%. Thus, although each pulse within a sequence could take on any value (or sign) from distribution $N(\mu_k, \sigma)$, the expectation of a sequence would be μ_k . Motion strength was then z scored over all sessions for each monkey separately.

On the motion strength axis, we use positive values to indicate motion towards the hemifield contralateral to the LIP under study, and negative values to indicate motion towards the hemifield ipsilateral to the LIP under study. We use the term ‘proportion choices’ to refer to the proportion of choices towards the contralateral target. For consistency, we maintain this convention throughout the paper, such that even on MT inactivations sessions, psychometric performance is evaluated in relation to the LIP under study.

The monkey was rewarded for selecting the target consistent with the sign of the motion pulse sequence sum (the net direction), independent of the distribution μ_k from which they were drawn. On trials that summed to exactly zero, the monkey was rewarded at random. 10% of trials consisted of a frozen random seed, generating identical pulse sequences. In addition to the direction discrimination task described here, we performed a subset of experiments ($n = 2$) using the classical moving dots stimulus¹⁵ with motion coherence values of 0, 3.2, 6.4, 12.8, 25.6 and 51.2% (Extended Data Fig. 6c).

Free-choice task. A free-choice task was used to measure spatial bias to one target over another and confirm a behavioural consequence of LIP inactivation^{8,21,35}. The task was performed before and after every LIP inactivation ($n = 21$ during experiments using the standard direction discrimination task, $n = 13$ during other experiments, see for example, Extended Data Fig. 6c). The sequence of events within the free-choice task is illustrated in Fig. 3a, b. Trials began with the appearance of a central fixation point. At a random time after acquiring fixation (500–900 ms), two targets were simultaneously flashed for a brief 200 ms. Subjects were required to maintain fixation until the fixation point disappeared (600 to 3,000 ms after target flash), and then saccade to either of the remembered locations of the two targets. On every trial, target position was determined independently from one another and at random, drawn from a 2D Gaussian with a mean of either (-12, 0)° (left target) or (12, 0)° (right), and a standard deviation of 2–4° for x and 3–5° for y position. Means and standard deviations were sometimes adjusted online to better position the distributions within the LIP receptive field (when recorded) or LIP inactivated field (when inactivated).

A trial was successfully completed when the monkey’s saccade entered a circular window (unobservable to the monkey) around either target and held for 300–500 ms (window radius scaled by $0.35 \times \text{eccentricity}$, minimum: 3°). Successfully completed free-choices were rewarded on 70% of trials irrespective of the target chosen for monkey N, and 100% of trials for monkey P. Monkey N also performed memory-guided saccades to single targets (30% of trials, randomly interleaved) that appeared randomly in space (uniform distribution), and were rewarded 100% of the time. The adjustments in subject N’s task were performed to prevent a spatial bias and encourage exploration. Overall performance and inactivation effects were similar between monkeys despite differences in task parameters. **Behavioural analysis.** All analyses were performed in MATLAB (MathWorks). Responses in the direction discrimination task were analysed with a maximum

likelihood fit of a two parameter logistic function³⁷ assuming a Bernoulli distribution of binary choices, in which the probability of a contralateral choice is P and ipsilateral choice is $1 - P$, where P is given by:

$$P = \frac{1}{1 + e^{-\beta(x-\alpha)}}$$

where x is the motion strength value (z -scored), α is the bias parameter (reflecting the midpoint of the function in units of motion strength), and β is the slope (that is, sensitivity, in units of log-odds per motion strength). Error estimates on the parameters were obtained from the diagonal of the inverse Hessian (second derivative matrix) of the negative log-likelihood. A four-parameter model including sub-perfect response rates for the top and bottom asymptotes⁸ was also considered, but did not confer any advantage over the two-parameter model nor change analysis results, and so we focused on the simpler two-parameter fit (Extended Data Table 1). The first 10–30 trials of every session were ‘instruction’ (or warm-up) trials (in which motion strength was set to maximal) and were excluded from analysis. Median session length for all baseline and treatment sessions was 409 trials. Sessions were excluded from analysis if the animal either completed less than 250 trials or performed poorly (lapse rate >10%). For inactivation sessions, all sessions were included regardless of performance. A single inactivation session in monkey P was aborted due to a leak in the infusion system, and was not included in the analysis.

Animal strategy in the direction discrimination task (Fig. 2f, g) was measured by computing psychophysical weights via logistic regression, where the probability of the binary choice $Y \in \{0,1\}$ on every trial is given by

$$p(Y|w, X) = e^{YXw} / (1 + e^{Xw})$$

where X is a matrix of the seven pulse values on each trial, augmented by a column to capture the bias term, and w is a vector of the monkey’s weights. We computed the maximum likelihood estimate of the weight vector w using MATLAB’s glmfit function.

In the free-choice task, spatial bias was computed as the proportion of choices to the target contralateral to the LIP under study. Saccade onset and offset were detected in every task by identifying the time at which eye velocity exceeded 30° per s (onset) and returned below 50° per s (offset). We only analysed saccades on trials where the task was completed successfully (no broken fixations and no saccades outside of the target windows). Saccades were analysed for reaction time, amplitude, duration, and error amplitude (distance of saccadic end point from saccadic target). Saccadic reaction times less than 100 ms from the go signal were excluded to ensure that only task relevant saccades are analysed.

Neuronal recordings. Recordings were performed in areas MT and LIP with either single-channel glass coated tungsten electrodes (Alpha Omega) or multi-electrode arrays (Plexon U or V Probe). Neuronal signals were amplified, band-pass filtered, digitized, and saved (Plexon MAP server). Neural waveforms passing a manually-set threshold were isolated for online mapping of their receptive fields (both MT and LIP) and directional tuning (MT).

MT receptive field locations were hand mapped using drifting dot stimuli in a circular aperture. Once the retinotopic location was identified, direction preference and selectivity were measured using drifting dot stimuli at 100% coherence in 12 directions. LIP receptive field locations were mapped with a memory-guided delayed saccade task³⁸.

In monkey P, offline spike sorting was performed by hand refinement of a standard clustering algorithm (Plexon Offline Sorter v3). Single unit isolation quality was established using SNR³⁹. In monkey N, spike sorting was performed by fitting a mixture of Gaussians model to clipped waveforms in a reduced dimensional space⁴⁰. In both monkeys, sorting was refined by maximum *a posteriori* estimation of a model, where the multi-electrode voltage was the linear superposition of Gaussian white noise and the spike waveforms^{41,42}.

Neuronal analysis. Peri-stimulus time histograms (PSTHs) were computed by aligning spike times to events (motion onset or saccade time), binned at 10 ms resolution, and smoothed with a Gaussian kernel with standard deviation of 25 ms. Trial motion strengths were binned into three groups: between 0 and 0.25, between 0.25 and 1, and greater than 1. We averaged spike rates separately for the three motion strengths for each choice. Note that these motion strengths correspond to a narrower range than that used in previous studies¹¹, selected to encourage longer integration times. This is evident in the PSTHs (narrow dynamic range) and psychometric functions (fewer data points in the asymptotic range of behaviour).

Choice probability. Choice probability is a metric used to measure the predictive relationship between neural responses and choice, independent of stimulus strength. It is defined as the area under the receiver operating characteristic curve (ROC) for a pair of spiking response distributions sorted by choice^{1,43}.

We quantified choice probability using trials that had zero expected motion and were repeated with identical random seeds (that is, had no stimulus variation, ‘frozen noise’). Sometimes more than one random seed was repeated in a session, in which case we calculated the spiking response distributions for each seed separately, subtracted the mean, and then combined them, similar to an analysis known as grand choice probability¹. Neurons with >20 frozen repeats were included (90/94 MT cells, 96/113 LIP cells), and significance testing against the null (that is, choice probability = 0.5) was performed using a Student’s t -test. In MT, we counted spikes during the motion epoch (1,050 ms). In LIP, we counted spikes over a 400 ms window counting backwards from the 100 ms before the saccade.

Infusion protocol. Infusions were performed by lowering an infusion cannula into grid locations that had previously yielded the largest number of selective cells during the recording phase of the study (Extended Data Fig. 1). The cannula (31–32 gauge) was lowered alongside a multi-electrode array, at least 1 mm away (Fig. 2a). The two were lowered to target cortical areas where functional identification took place (mapping). Infusion was then performed, and electrophysiological silencing was confirmed on the recording electrodes, typically within 15 min of infusion start.

Infusions were performed with a syringe pump (Harvard Apparatus) through a single and direct line to the cannula (constant rate of 0.1–0.4 $\mu\text{l min}^{-1}$, 15–30 min), in agreement with infusion parameters proposed in ref. 44. We delivered 6.66–8 $\mu\text{g } \mu\text{l}^{-1}$ muscimol (in phosphate buffered saline) at volumes of 5–12 μl (mean 7.4 μl), netting a total mass of 40–80 μg (mean 56.4 μg). This protocol was chosen to match the very high end of ranges used previously in order to maximize neural inactivation. Infusions were typically made at multiple depths within a single cannula track. On 5 of the 21 main LIP inactivation sessions, more than one cannula was lowered (Extended Data Table 2). Cannulae were left *in situ* for at least 15 min after infusion end. Saline infusions followed the same protocol and included both a cannula and multi-electrode array. Sham infusions included only a multi-electrode array but followed similar timings, including the operation of the syringe pump with no syringe attached.

Spatial and temporal extent of inactivation. Previous analyses of the spatial extent of muscimol inactivation have estimated the functional silencing to cover a spherical radius of roughly 2–3 mm^{34,45–47}. The study most comparable to ours, by Liu *et al.*³⁴, co-infused muscimol and Manganese (Mn) into LIP of awake macaques and imaged the spread. They also estimated a cortical silencing of approximately 2–3 mm in radius, consistent with the linear dependence of volume distribution (mm^3) on infusion volume (μl)⁴⁸.

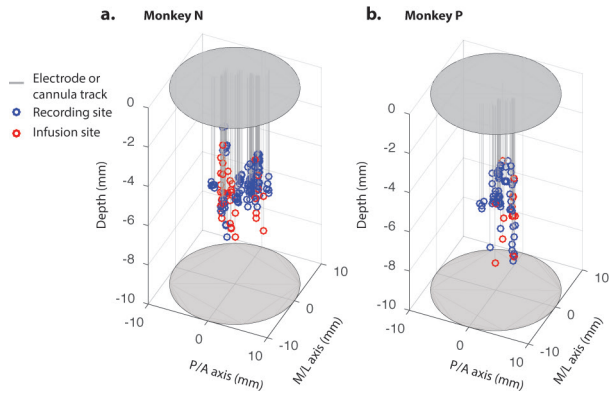
In our experiments, lowering both a multi-electrode array and infusion cannula collaterally (Fig. 2b) enabled direct confirmation of neural silencing at known distances from the cannula tip. This places a lower bound on the spatial extent of functional inactivation. Although our standard protocol placed the multi-electrode array 1 mm away from the cannula tip, we sometimes lowered a second array, 2 or 3 mm away. On these sessions too, we observed silencing on most recording channels. Taken together, we conservatively estimate neural inactivation in LIP to span a radius of at least 2.5 mm, silencing large swaths of LIP, while primarily targeting its ventral portion^{34,49}. For inactivations of this spatial magnitude, there is no evidence that larger inactivations result in larger behavioural deficits²⁰. Similarly, we did not observe a dose–response function in our own data (Extended Data Fig. 3c–e).

On a few occasions, residual firing persisted despite near-complete silencing of electrophysiological activity (example shown in Fig. 2b, voltage traces, channels 5 and 6). We tested the selectivity of residual firing with the appropriate mapping task (motion for MT, memory guided saccades for LIP) and found that these spikes did not respond selectively, indicating that these residual spikes likely emanate from afferent fibres terminating within the inactivated area⁵⁰.

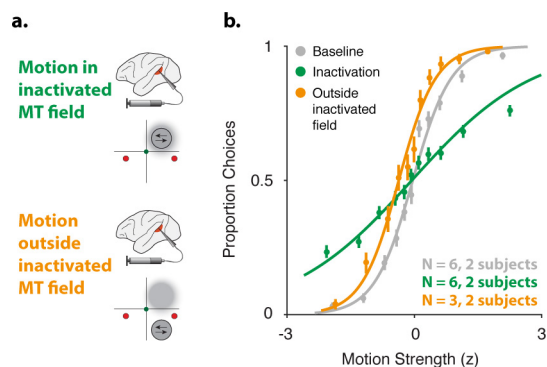
Previous LIP inactivation studies found no evidence to support within-session compensation that manifests behaviourally^{19,20,34,47,51}, but see ref. 21. Studies that report the temporal effect of LIP inactivation find an increase in the impact over time, not a decrease^{19,51}. Regardless, we explored the time course of psychophysical performance within a session (Extended Data Fig. 4), and also evaluated compensation on longer time scales, across sessions, to explore the possibility of increasing behavioural robustness to inactivation that might develop over time (Extended Data Fig. 5).

31. Meister, M. L. R., Hennig, J. A. & Huk, A. C. Signal multiplexing and single-neuron computations in lateral intraparietal area during decision-making. *J. Neurosci.* **33**, 2254–2267 (2013).
32. Brainard, D. H. The Psychophysics Toolbox. *Spat. Vis.* **10**, 433–436 (1997).
33. Eastman, K. M. & Huk, A. C. PLDAPS: a hardware architecture and software toolbox for neurophysiology requiring complex visual stimuli and online behavioral control. *Front. Neuroinform.* **6**, 1 (2012).
34. Liu, Y., Yttri, E. A. & Snyder, L. H. Intention and attention: different functional roles for LIPd and LIPv. *Nature Neurosci.* **13**, 495–500 (2010).

35. Zirnsak, M., Chen, X., Lomber, S. G. & Moore, T. Effects of reversible inactivation of parietal cortex on the processing of visual salience in the frontal eye field. *Proc. Conference Soc. Neurosci.* (2015).
36. Patel, G. H. *et al.* Topographic organization of macaque area LIP. *Proc. Natl Acad. Sci. USA* **107**, 4728–4733 (2010).
37. Wichmann, F. A. & Hill, N. J. The psychometric function: I. Fitting, sampling, and goodness of fit. *Percept. Psychophys.* **63**, 1293–1313 (2001).
38. Gnadt, J. W. & Andersen, R. A. Memory related motor planning activity in posterior parietal cortex of macaque. *Exp. Brain Res.* **70**, 216–220 (1988).
39. Kelly, R. C. *et al.* Comparison of recordings from microelectrode arrays and single electrodes in the visual cortex. *J. Neurosci.* **27**, 261–264 (2007).
40. Tolias, A. S. *et al.* Recording chronically from the same neurons in awake, behaving primates. *J. Neurophysiol.* **98**, 3780–3790 (2007).
41. Pillow, J. W. *et al.* Spatio-temporal correlations and visual signalling in a complete neuronal population. *Nature* **454**, 995–999 (2008).
42. Pillow, J. W., Shlens, J., Chichilnisky, E. J. & Simoncelli, E. P. A model-based spike sorting algorithm for removing correlation artifacts in multi-neuron recordings. *PLoS One* **8**, e62123 (2013).
43. Celebrini, S. & Newsome, W. T. Neuronal and psychophysical sensitivity to motion signals in extrastriate area MST of the macaque monkey. *J. Neurosci.* **14**, 4109–4124 (1994).
44. Noudoost, B. & Moore, T. A reliable microinjector system for use in behaving monkeys. *J. Neurosci. Methods* **194**, 218–223 (2011).
45. Martin, J. H. Autoradiographic estimation of the extent of reversible inactivation produced by microinjection of lidocaine and muscimol in the rat. *Neurosci. Lett.* **127**, 160–164 (1991).
46. Arikian, R. *et al.* A method to measure the effective spread of focally injected muscimol into the central nervous system with electrophysiology and light microscopy. *J. Neurosci. Methods* **118**, 51–57 (2002).
47. Yttri, E. A., Wang, C., Liu, Y. & Snyder, L. H. The parietal reach region is limb specific and not involved in eye-hand coordination. *J. Neurophysiol.* **111**, 520–532 (2014).
48. Heiss, J. D., Walbridge, S., Asthagiri, A. R. & Lonser, R. R. Image-guided convection-enhanced delivery of muscimol to the primate brain. *J. Neurosurg.* **112**, 790–795 (2010).
49. Lewis, J. W. & Van Essen, D. C. Mapping of architectonic subdivisions in the macaque monkey, with emphasis on parieto-occipital cortex. *J. Comp. Neurol.* **428**, 79–111 (2000).
50. Chapman, B., Zahs, K. R. & Stryker, M. P. Relation of cortical cell orientation selectivity to alignment of receptive fields of the geniculocortical afferents that arborize within a single orientation column in ferret visual cortex. *J. Neurosci.* **11**, 1347–1358 (1991).
51. Kubanek, J., Li, J. M. & Snyder, L. H. Motor role of parietal cortex in a monkey model of hemispatial neglect. *Proc. Natl Acad. Sci. USA* **112**, E2067–E2072 (2015).

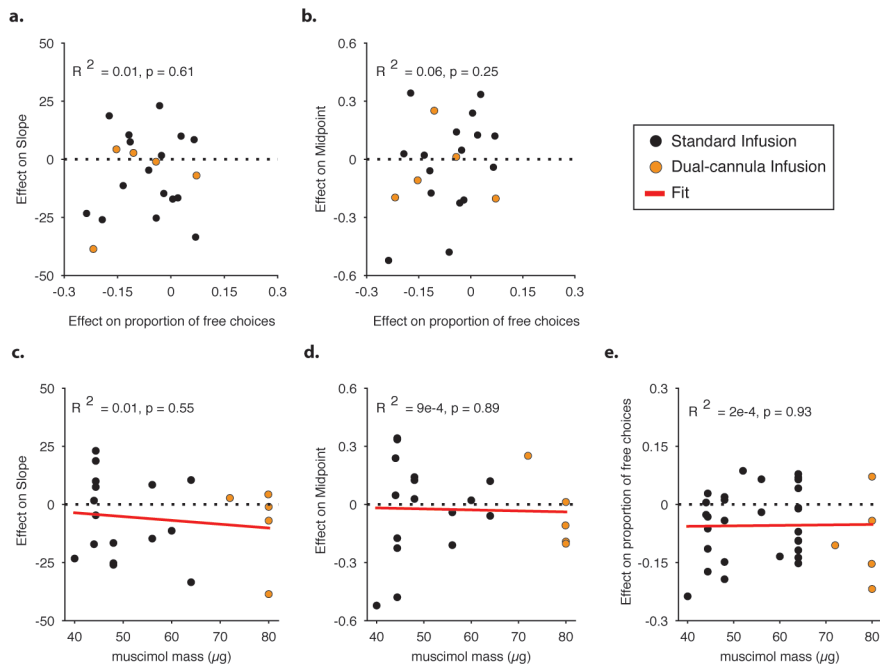


Extended Data Figure 1 | Location of LIP recording and muscimol infusion sites. a, b, The recording (blue circles) and infusion sites (red) for monkey N (**a**) and monkey P (**b**) along the medial-lateral (M/L) and posterior-anterior (P/A) axes within the chamber (demarcated by the ovals). Electrode and cannula tracks are represented by the grey lines (with a small jitter on the x - y plane for better visualization). The mean infusion depths were 7.12 ± 1.15 mm (monkey N) and 7.03 ± 1.39 mm (monkey P) (the microdrive was zeroed below dura mater and just above the cortical surface). Given the estimated spread of muscimol described in the main text, the inactivations targeted a substantial territory of the ventral portion of LIP⁴⁹. Even though a functional distinction with depth has been proposed³⁴, we emphasize that the critical component of our protocol was targeting the precise locations at which we measured canonical decision-related activity in LIP.



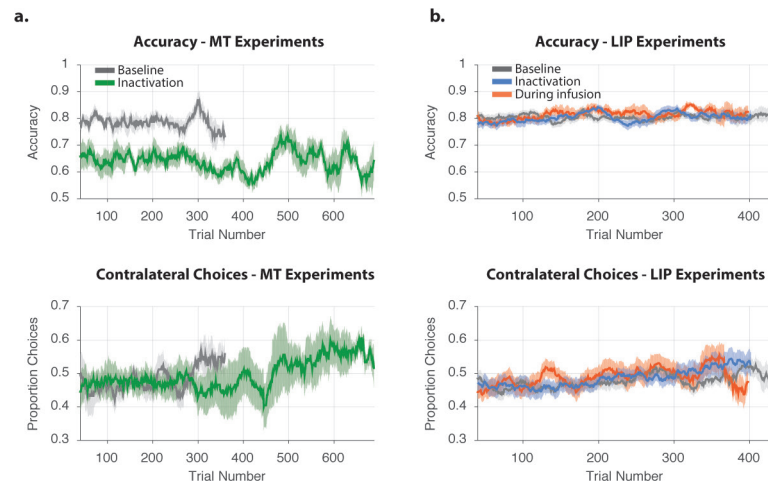
Extended Data Figure 2 | Direction discrimination sensitivity is restored when motion is placed outside of the inactivated MT field.

a. Illustration of MT inactivation along with the estimated inactivated field (grey cloud), for two experimental geometries: motion stimulus placed inside the inactivated MT field (top) and motion placed outside the inactivated MT field (bottom). **b.** Average psychophysical data for baseline and muscimol treatment pairs (grey and green, respectively, same data as Fig. 2c, $n = 6$; 3 in monkey N; 3 in monkey P) and psychophysical data collected during muscimol treatment, with the motion stimulus outside of the inactivated MT field (orange, $n = 3$). Direction discrimination sensitivity is restored to baseline levels in these sessions. Error bars on points show ± 1 s.e.m. over all trials.



Extended Data Figure 3 | No relationship between effect magnitude in control task, effect magnitude in direction discrimination task, and muscimol mass. **a, b,** The relationship between the effect of LIP inactivation in the free-choice task (that is, shift in proportion of contralateral choices from baseline to muscimol treatment) and the effect of LIP inactivation in the direction discrimination task on sensitivity (percentage change in psychometric function slope, **a**) and bias (shift in normalized motion strength, **b**). R^2 and associated P values of a Pearson correlation are indicated on individual plots ($n = 21$; 12 in monkey N; 9 in monkey P). Orange data points indicate sessions in which muscimol

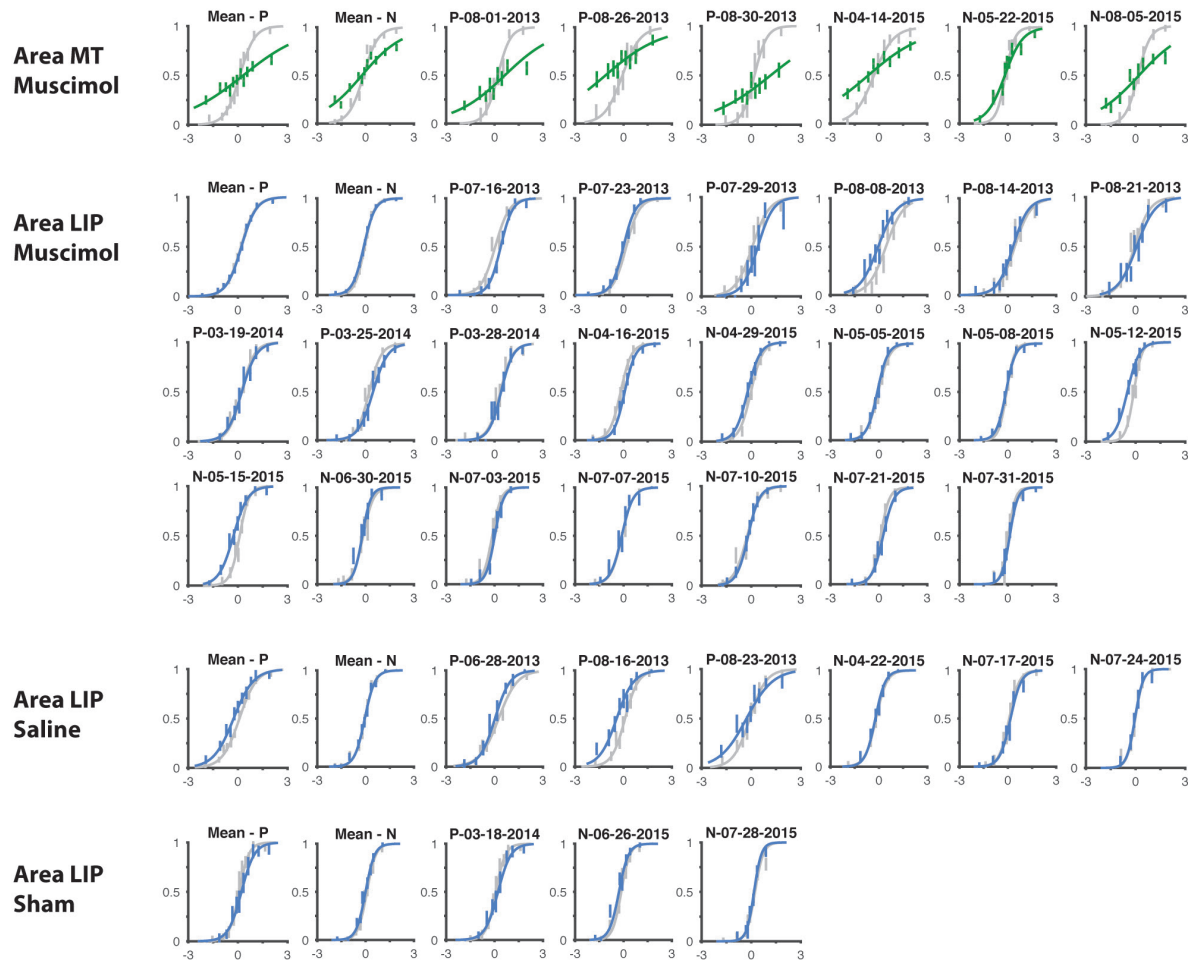
was infused from two cannulae simultaneously into LIP. **c–e,** Dose–response functions between muscimol mass and the effect in the direction discrimination task on slope (**c**, same units as **a**), bias (**d**, same units as **b**), and the effect in the free-choice task (**e**, same units as **a, b**). For **e**, we used free-choice sessions that took place on the same days as the direction discrimination task ($n = 21$) along with an additional 13 sessions that took place during other inactivation experiments under similar conditions ($n = 34$ in total; 14 in monkey N; 20 in monkey P; as in Fig. 3d). R^2 , associated P values and regression lines are indicated on the plots (linear regression).



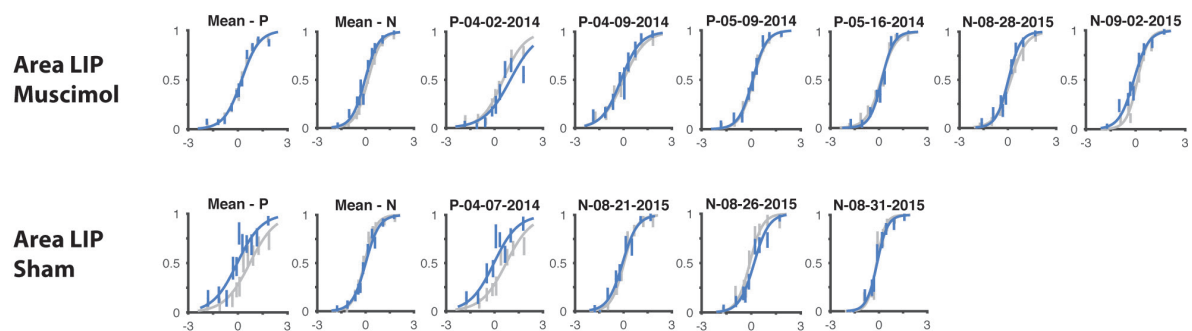
Extended Data Figure 4 | Time course of accuracy and bias within sessions. Accuracy and bias in the direction discrimination task were computed over time by taking a running mean of correct and contralateral choices, respectively (sliding window of 40 trials). **a**, Inactivation in area MT ($n = 6$, green curve; 3 in monkey N; 3 in monkey P) had a clear and consistent impact on behavioural accuracy compared to baseline ($n = 6$, grey), but did not have systematic effects on bias (bottom), consistent with our results from the fitted psychometric functions (main text). Panels show data from trial 40 (sliding window size) to the median trial length of each group of experiments (variable session lengths contribute to increased variability at later trials). Error bars show ± 1 s.e.m. between sessions. **b**, Inactivations in area LIP ($n = 21$, blue curve; 12 in monkey N;

9 in monkey P) yielded no systematic trends in either accuracy (top) or bias (bottom) compared to baseline ($n = 21$, grey), indicating that within-session compensation is unlikely. Panel format same as in **a**. We also investigated whether compensation may have taken place before we began collecting the ‘inactivation’ data set, or during the first 10–30 instruction (warm-up) trials. On 13 of the 21 LIP inactivation sessions, we collected a third data set (in addition to the standard paired baseline and inactivation data sets), in which psychophysical performance was monitored during the time muscimol was being infused (during infusion, orange curve). No systematic changes in accuracy or bias were observed in this exploratory data set either, further arguing against compensation on the time scales of our manipulations and measurements.

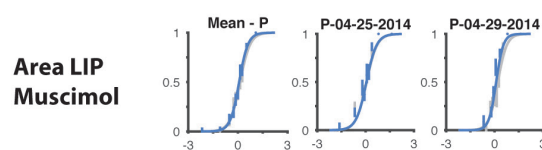
a. Standard Geometry



b. Both targets in inactivated field



c. Newsome dots



Extended Data Figure 6 | Psychophysical performance for all individual baseline and treatment session pairs. a–c. All pairs of baseline and treatment sessions for all treatment types: muscimol, saline, and sham, (control pairs with no saline/sham manipulation are similar but not presented, for visual clarity) for all variants of the direction discrimination task: standard geometry (a), both targets in inactivated field (b), and Newsome dots (c), for both LIP and MT inactivation. In all panels, the

abscissa represents motion strength towards the direction contralateral to the LIP under study, the ordinate represents the proportion of contralateral choices. The grey curve is baseline, and the coloured curve is treatment. The first panel in each section presents mean psychophysical performance for each monkey over sessions. Subsequent panels present individual session pairs. Error bars are s.e.m. over all trials.

Extended Data Table 1 | Parametric and nonparametric analysis of psychophysical data, for two- and four-parameter psychometric functions

Statistical		Muscimol Infusions				Control Infusions				Muscimol vs. Control Infusions				
test	model monkey	midpoint	slope	minLapse	maxLapse	midpoint	slope	minLapse	maxLapse	midpoint	slope	minLapse	maxLapse	
Student's t	pmf2	N	0.542	0.1734			0.986	0.2444			0.149	0.2367		
		P	0.6731	0.7982			0.2353	0.2166			0.0208	0.2461		
		Both	0.9306	0.1659			0.3693	0.1092			0.2606	0.0704		
	pmf4	N	0.4028	0.0243	0.7585	0.2352	0.8213	0.2827	0.6065	0.6228	0.8213	0.2827	0.6065	0.6228
		P	0.6747	0.459	0.3554	0.8337	0.1377	0.3261	0.5675	0.3111	0.1377	0.3261	0.5675	0.3111
		Both	0.8163	0.0552	0.3904	0.9091	0.2169	0.1595	0.7461	0.2734	0.2169	0.1595	0.7461	0.2734
WSRST	pmf2	N	0.791	0.3394			0.9308	0.2305			0.184	0.1496		
		P	0.5703	0.9102			na	na			0.0503	0.3301		
		Both	0.9032	0.3219			0.4432	0.1036			0.3898	0.0324		
	pmf4	N	0.6221	0.021	0.5186	0.2334	0.9032	0.2305	0.3754	0.4761	0.184	0.4887	0.184	0.5125
		P	0.4961	0.4258	0.8203	0.8203	na	na	0.875	0.625	0.0503	0.6042	0.8252	0.8252
		Both	0.8213	0.0325	0.414	0.566	0.3533	0.1353	0.2758	0.3674	0.3543	0.0895	0.4942	0.2009

The entries show *P* values for two types of statistical analyses: the parametric Student's *t*-test and the non-parametric Wilcoxon signed-rank sum test (WSRST). The tests were performed on model parameters fit to individual sessions. We present data for the standard two-parameter psychometric function (pmf2), and for an exploratory four-parameter psychometric function (pmf4). Muscimol infusions: paired tests compared muscimol baseline sessions to muscimol treatment sessions. Control infusions: paired tests compared saline/sham/control baseline sessions to saline/sham/control treatment sessions. Muscimol versus control infusion: unpaired tests compared muscimol treatment sessions to saline/sham/control treatment sessions. na, not enough data.

Extended Data Table 2 | Infusion details for all treatment sessions

Task	Area	Monkey	Date	Treatment	Cannula Tracks (#)	Positioning Grid (x, y)	Infusion sites within Track (#)	Average depth (mm)	Total volume (μ l)	Total mass (μ g)
Standard task geometry	MT	P	20130801	Muscimol	1	(2, -1)	2	8	5	33.3
			20130826	Muscimol	1	(2, 0)	2	10	9.7	64.3
			20130830	Muscimol	1	(2, 0)	2	11.2	8.5	56.6
	N	20150414	Muscimol	1	(5, -4)	3	10.7	4	32	
		20150522	Muscimol	1	(5, -4)	2	10.5	5	40	
		20150805	Muscimol	1	(4, -4)	2	6.9	5	40	
LIP	P	20130628	Saline	1	(2, -1)	1	7	6.7	-	
		20130716	Muscimol	1	(3, 0)	1	6.5	6.7	44.4	
		20130723	Muscimol	1	(3, 0)	1	7	6.7	44.4	
		20130729	Muscimol	1	(2, -1)	1	7	6.7	44.4	
		20130808	Muscimol	1	(3, 0)	1	6	6.7	44.4	
		20130814	Muscimol	1	(3, 0)	1	7	6.7	44.4	
		20130816	Saline	1	(3, 0)	1	6	6.7	-	
		20130821	Muscimol	2	(3, 0); (0, 3)	2; 2	7; 7	12	79.9	
		20130823	Saline	1	(3, 0)	1	7	6.7	-	
		20140318	Sham	-	-	-	-	-	-	
		20140319	Muscimol	1	(3, 0)	1	7	5	40	
		20140325	Muscimol	1	(3, 0)	1	7	6	48	
		20140328	Muscimol	2	(3, 0); (1, -3)	2; 2	7.5; 7.5	10	80	
		N	20150416	Muscimol	1	(2, 4)	2	6.3	6	48
			20150422	Saline	1	(2, 4)	1	7.6	5	-
	20150429		Muscimol	1	(-2, 3)	2	6.6	7.5	60	
	20150505		Muscimol	1	(-2, 3)	2	6.5	5.5	44	
	20150508		Muscimol	1	(-1, 3)	2	8.6	5.5	44	
	20150512		Muscimol	2	(-2, 3); (3, 4)	2; 2	7.9; 7.9	9	72	
	20150515		Muscimol	1	(-2, 3)	3	7.6	7	56	
	20150626		Sham	-	-	-	-	-	-	
	20150630		Muscimol	1	(-2, 3)	2	8	7	56	
	20150703		Muscimol	1	(-3, 2)	3	7.1	8	64	
	20150707		Muscimol	2	(-3, 2); (2, 4)	3; 3	7.9; 7.9	10	80	
	20150710		Muscimol	2	(-3, 2); (2, 3)	2; 2	6.2; 6	10	80	
	20150717		Saline	1	(-3, 2)	2	5.3	6	-	
	20150721		Muscimol	1	(-3, 2)	2	6.1	8	64	
	20150724		Saline	1	(-3, 2)	2	6	5	-	
	20150728		Sham	-	-	-	-	-	-	
	20150731	Muscimol	1	(-3, 2)	3	6	6	48		
	Both targets in inactivated field	LIP	P	20140402	Muscimol	1	(3, 0)	2	7.5	6
20140407				Sham	-	-	-	-	-	-
20140409				Muscimol	1	(3, 0)	4	7	8	64
20140509				Muscimol	1	(3, 0)	3	9	8	64
20140516				Muscimol	1	(3, 0)	3	9	8	64
N		20150821	Sham	-	-	-	-	-	-	
		20150826	Sham	-	-	-	-	-	-	
		20150828	Muscimol	1	(-3, 2)	3	7	6	48	
		20150831	Sham	-	-	-	-	-	-	
		20150902	Muscimol	1	(-3, 2)	4	6.2	6.5	52	
Newsome Dots	LIP	P	20140425	Muscimol	1	(3, 0)	3	7.2	8	64
			20140429	Muscimol	1	(3, 0)	3	7.6	8	64

The table presents all infusion sessions run over the course of the study for all infusion types (muscimol, saline, sham), in either MT or LIP. Infusions are sorted by date within each task, for each monkey separately. Positioning grid values are relative to chamber centres (see Methods for stereotactic coordinates). Average depth refers to the average depth across all infusion sites within a given cannula track. Total volume and total mass refer to the sum over all infusion sites and tracks.